Endothelial NOD1 directs myeloid cell recruitment in atherosclerosis through VCAM-1

Silvia González-Ramos[1,2]; Marta Paz-García[1,2]; Cristina Rius[3§]; Alberto del Monte-Monge[3,2§]; Cristina Rodríguez[4,2]; Victoria Fernández-García[1,2]; Vicente Andrés[2,3]; José Martínez-González[2,5]; Miguel A. Lasunción[6]; Paloma Martín-Sanz[1,2]; Oliver Soehnlein[7,8, 9]*; Lisardo Boscá[1,2*,#].

[1]Instituto de Investigaciones Biomédicas Alberto Sols (CSIC-UAM), Madrid, Spain; [2]Centro de Investigación Biomédica en Red en Enfermedades Cardiovasculares (CIBER-CV), Madrid, Spain; [3]Centro Nacional de Investigaciones Cardiovasculares (CNIC), Madrid, Spain; [4]Institut de Recerca del Hospital de la Santa Creu i Sant Pau-Programa ICCC, IIB Sant Pau, Barcelona, Spain; [5]Instituto de Investigaciones Biomédicas de Barcelona (CSIC-IIBB), IIB Sant Pau, Barcelona, Spain; [6]Hospital Universitario Ramón y Cajal (IRyCIS), CIBEROBN, Madrid, Spain; [7]Institute for Cardiovascular Prevention, Ludwig-Maximilians-University (LMU), Munich, Germany; [8]Karolinska Institutet, Stockholm, Sweden; [9]German Center for Cardiovascular research (DZHK), partner site Munich Heart Alliance (MHA), Berlin, Germany.

Running title: Endothelial NOD1 directs myeloid cell recruitment

Address correspondence to:

Lisardo Boscá

Instituto de Investigaciones Biomédicas Alberto Sols

C/Arturo Duperier, 4

28029 Madrid

Phone +34-(0)91-497-2747

Email lbsoca@iib.uam.es

or

Oliver Soehnlein

Institute for Cardiovascular Prevention

Ludwig-Maximilians-University Munich

Pettenkoferstr. 9

80336 Munich

Phone +49-(0)89-4400-54667

Email oliver.soehnlein@gmail.com

§These authors contributed equally to this work.
*OS and LB contributed equally as corresponding and senior authors.
#Lead Contact

Nonstandard abbreviations

ADES   Aorta dissociation enzyme solution

BM   Bone marrow

CAD   Coronary artery disease

EC   Endothelial cell

ECAM   Endothelial cell adhesion molecule

FDG   Fluorodeoxyglucose

HE   Haematoxylin-eosin

HFD   High-fat diet

iE-DAP   γ-D-glutamyl-meso-diaminopimelic acid

MLEC   Murine lung endothelial cell

NLR   Nucleotide-binding leucine-rich repeat-containing receptor

ORO   Oil Red O

oxLDL   Oxidised low-density lipoprotein

PGN   Peptidoglycan

PRR   Pattern-recognition receptor

SUV   Standardized uptake value

TBR   Target-to-background ratio

VEGF   Vascular endothelial growth factor

Abstract

Atherosclerosis is a chronic disease characterized by vascular lipid retention and inflammation, and pattern recognition receptors (PRRs) are important contributors in early stages of the disease. Given the implication of the intracellular PRR NOD1 in cardiovascular diseases, we investigated its contribution to early atherosclerosis. We evidenced NOD1 induction in atherosclerotic human and mouse tissues, predominantly in vascular endothelial cells (ECs). Accordingly, NOD1 genetic inactivation in *Apoe*$^{-/-}$ mice reduced not only atherosclerosis burden, but also monocyte and neutrophil accumulation in atheromata. Of note, in presence of either peptidoglycan or oxidized LDLs, endothelial NOD1 triggered VCAM-1 upregulation through the RIP2-NF-κB axis in an autocrine manner, enhancing firm adhesion of both sets of myeloid cells to the inflamed micro- and macro-vasculature *in vivo*. Our data define a major pro-atherogenic role for endothelial NOD1 in early leukocyte recruitment to the athero-prone vasculature, thus introducing NOD1 as an innovative therapeutic target and potential prognostic molecule.

Keywords: cardiovascular disease / innate immunity / leukocyte recruitment / endothelial cell adhesion molecule / pattern recognition receptors

INTRODUCTION

The *response-to-injury* theory poses that endothelial dysfunction as a consequence of disturbed flow, as well as exposure to noxious stimuli, represents the initial event in the pathogenesis of atherosclerosis (1). This endothelial dysfunction enhances endothelial permeability to atherogenic lipoproteins (mainly apolipoprotein B-containing low-density lipoproteins, LDLs) and activation of endothelial cell adhesion molecules (ECAMs) to promote infiltration of leukocytes to the subendothelial space. The most relevant ECAMs in leukocyte arrest belong to the immunoglobulin superfamily of adhesion molecules (Ig-CAMs). In this regard, endothelial vascular cell-adhesion molecule 1 (VCAM-1) binds to the integrin cell-surface ligand very late antigen 4 (VLA-4) in monocytes and T-cells preferably, meanwhile neutrophils use the endothelial intracellular adhesion molecule 1 (ICAM-1) to transiently bind to its ligand lymphocyte function-associated antigen 1 (LFA-1) (2).

Although the best-known danger signal in human atherosclerosis is oxidised LDL (oxLDL) (3), the atherosclerotic lesion contains a mixture of pattern-recognition receptor (PRR) ligands also implicated in the inflammatory response in the vessel wall (4). The cytoplasmic PRR nucleotide-binding oligomerization domain (NOD)-1 receptor, is a family member of the nucleotide-binding leucine-rich repeat-containing receptors (NLRs). To date, two NOD-containing molecules, NOD1 (CARD4) and NOD2 (CARD15), have been identified. Although both receptors detect bacterial peptidoglycan (PGN) fragments, NOD1 senses a conserved region of PGN (γ-D-glutamyl-*meso*-diaminopimelic acid, iE-DAP) common to almost all Gram-negative and some Gram-positive bacteria (5). Upon recognition of PGN, NOD1 and NOD2 homodimerise and interact with the receptor interacting protein-2 (RIP2 or RICK). This essential adaptor molecule is a serine/threonine kinase that through the assembly to large multi-protein complexes (including the IκB kinase (IKK) complex) lately activates the canonical nuclear factor kappa B (NF-κB) signalling pathway (6–8).

Here we determined the role of NOD1 in atherosclerosis-related endothelial dysfunction. Our results indicate that NOD1 in presence of oxLDL or PGN, induces an autocrine response in the vascular endothelium that promotes early atherosclerosis through VCAM-1 upregulation and concomitant monocyte and neutrophil recruitment to the vasculature.

MATERIALS & METHODS

Human samples

Human coronary arteries were collected from patients undergoing heart transplant at the Hospital de la Santa Creu i Sant Pau (Barcelona, Spain). Atherosclerotic and non-atherosclerotic coronary arteries were from coronary artery disease (CAD) and non-CAD patients, respectively. Written consent was obtained from all participating subjects. The studies were approved by the Ethics Committee and were conducted in accordance with the Helsinki Declaration.

Mouse models

Animal studies were approved by the local ethics committee, and all animal procedures conformed to EU Directive 2010/63 and Recommendation 2007/526/EC regarding the protection of animals used for experimental and other scientific purposes, enforced in Spanish law under Real Decreto 53/2013.

C57BL/6 (*Wt*) and *Apoe*$^{-/-}$ mice (9, 10) were obtained from Charles River (JAX mice stock #000664 and #002052, respectively). The homozygous *Nod1*$^{-/-}$ mice (mixed C57BL/6 and 129/C57BL/6 background), had been previously described (11) and were kindly gifted from Dr. Gabriel Núñez (University of Michigan Health System, UMHS, Michigan, USA).

Double-knockout *Apoe*$^{-/-}$*Nod1*$^{-/-}$ mice were generated by crossing *Apoe*$^{-/-}$ mice with *Nod1*$^{-/-}$ mice. Heterozygous mice were intercrossed to generate homozygous *Apoe*$^{-/-}$ bearing combinations of *Nod1*$^{+/+}$ and *Nod1*$^{-/-}$ mice at the expected mendelian ratio. All mice were genotyped by polymerase chain reaction (PCR) from ear samples using standard procedures. The absence of NOD1 expression in cells from *Apoe*$^{-/-}$*Nod1*$^{-/-}$ mice was confirmed by reverse transcriptase-polymerase chain reaction analysis (data not shown).

All experiments compared male *Apoe*$^{-/-}$ mice to male *Apoe*$^{-/-}$*Nod1*$^{-/-}$ littermates. In order to accelerate the development of atherosclerotic lesions, at 12 weeks of age, males were placed on high-fat diet (HFD, 10.7% total fat, 0.75% cholesterol; Sniff, Soest, Germany) for 3 weeks.

Mouse Lung Endothelial Cells isolation and culture

One of the greatest sources of endothelial cells (ECs) is the pulmonary endothelium, a continuous endothelial monolayer on the luminal surface of the lung vasculature. Therefore, to boost the yield of primary endothelial cells isolation, we isolated murine lung endothelial cells (MLECs) from male *Wt*, *Nod1*$^{-/-}$, *Apoe*$^{-/-}$*Nod1*$^{-/-}$ and *Apoe*$^{-/-}$ lungs by positive selection using mouse anti-CD102 antibody (BD Biosciences, San Jose, CA, USA) bound to magnetic beads (Dynabeads®, Invitrogen, Waltham, MA, USA) as described previously (12).

Subconfluent primary cell cultures underwent then a second round of positive selection using mouse anti-CD31 antibody (BD Biosciences, San Jose, CA, USA). The endothelial cell culture purity was further assessed by flow cytometry (FACSCanto II; Becton Dickinson, Franklin Lakes, NJ, USA) for endothelial

cell surface markers (VCAM-1 –R&D, Minneapolis, MN, USA- and CD54 -BD Biosciences, San Jose, CA, USA-) using standard procedures. This procedure resulted in a ≥99% pure population of endothelial cells. MLECs were grown on 0.1% gelatine (Sigma, St. Louis, MO, USA) in low-glucose DMEM-F12 (Sigma, St. Louis, MO, USA) supplemented with 20% FBS, endothelial cell growth supplement (ECGS, 50 µg/mL, Sigma, St. Louis, MO, USA) and antibiotics (100 units/mL penicillin and 100 µg/mL streptomycin).

When indicated, MLECs were pre-incubated with 1 µM Nodinitib-1 (Cayman, Ann Arbor, Michigan, USA), 5 µM BAY 11-7082 (Merck Millipore, Ontario, Toronto, Canada), 5 µM GSK583 (Cayman, Ann Arbor, Michigan, USA) or 1 µg/mL LOX1 neutralizing antibody (Abcam, Cambridge, UK) for one hour and then treated with 50 µg/mL LDL, 50 µg/mL oxidized LDL (Biochemistry-Research Unit at *Instituto Ramón y Cajal de Investigación Sanitaria*, Spain), 10 ng/mL mouse TNF-α (PeproTech, London, UK), 1 µg/mL iE-Lys or 1 µg/mL C12-iE-DAP (Invivogen, San Diego, CA, USA) for 24 hours. For co-culture assays, cell-free MLEC supernatants were collected after 24 hours stimulation and directly transferred to non-stimulated MLEC subconfluent monolayers.

qRT-PCR

Total RNA was isolated by homogenization in QUIAZOL® by a TissueLyser LT and eluted using MinElute columns (Qiagen, Germantown, MD, USA). RNA integrity was assessed by RNA Nano Chip (Agilent Technologies, Santa Clara, CA, USA). 250 ng of RNA were retro-transcribed by using High-Capacity cDNA Reverse Transcription Kit (Applied Biosystems, Foster City, CA, USA) and qRT-PCR was conducted in 7900HT Fast Real-Time PCR System equipment using a Taqman Gene Expression Assay specific for mouse *Nod1* (1308180) and *18S* (4352930E) (Applied Biosystems, Foster City, CA, USA). SYBR Green was used for qRT-PCR detection of *Nod2* (5'-TGGACACAGTCTGGAACAAGG-3' and 5'-CAGGACCCATACAGTTCAAAGG-3'), *Lox1* (5'-CAAGATGAAGCCTGCGAATGA-3' and 5'-ACCTGGCGTAATTGTGTCCAC-3') and *18S* (5'-CCAGTAAGTGCGGGTCATAAGC-3' and 5'-CCTCACTAAACCATCCAATCGG-3').

Calculations were made from measurement of technical triplicates of each sample. The relative amount of mRNA was calculated with the comparative $2^{-\Delta\Delta Ct}$ method using mouse *18S* or *36b4* as endogenous control transcripts.

Western blot analysis

Human specimens and mouse aortic samples for western blotting were snap-frozen in liquid nitrogen and stored at -80ºC. Human protein extracts were obtained using ice-cold lysis buffer containing 50 mM Tris-HCl pH 7.5, 1% (w/v) Triton X-100, 150 mM NaCl and 1 mM DTT, supplemented with phosphatase cocktail and protease inhibitors (Sigma, St. Louis, MO, USA) (13). Mouse tissue and MLECs whole protein extracts were obtained using ice-cold proprietary detergent in 25 mM bicine, 150 mM sodium chloride; pH

7.6 (T-PER® Tissue Protein Extraction Reagent, Thermo Sci., Waltham, MA, USA) supplemented with same phosphatase and protease inhibitors.

Proteins were resolved on SDS-PAGE gels and then transferred to nitrocellulose membranes. Proteins were detected using rabbit polyclonal antibody against NOD1 (1:500, Abcam, Cambridge, UK), rabbit monoclonal antibody against phospho-RIP2 (1:1000, Cell Signaling, Danvers, MA, USA), rabbit polyclonal antibody against phospho-RIP2 (1:1000, Cell Signaling, Danvers, MA, USA), rabbit polyclonal antibody against phospho-NF-κB (1:1000, Santa Cruz, Dallas, Texas, USA), mouse monoclonal antibody against GAPDH (1:10000, Thermo Sci., Waltham, MA, USA), mouse monoclonal antibody against β-actin (1:40000, Sigma, St. Louis, MO, USA), mouse monoclonal antibody against α-tubulin (1:10000, Sigma, St. Louis, MO, USA) and HRP-conjugated secondary antibodies (Biorad, Hercules, CA, USA).

Protein bands were visualized using a Luminata® chemiluminescence detection system (Merck Millipore, Ontario, Toronto, Canada) and a ImageQuant LAS 500 imager (GE Healthcare Life Sci., Freiburg, Germany) and were quantified using ImageJ (National Institutes of Health, NIH, Bethesda, Maryland, USA). Intensities of the NOD1 and pRIP2 bands were expressed as a percentage of those of the GAPDH or β-actin bands as indicated.

Lesion quantification

After mouse cardiac perfusion with PBS supplemented with 5 mM of EDTA, mouse hearts were harvested and fixed in 4% paraformaldehyde (PFA) for 24 h at 4° C, incubated 24 h in PBS supplemented with 30% sucrose, embedded in OCT and cryopreserved at -70ºC.

Cryocut cross-sections (5-µm) of aortic roots were evaluated for conventional haematoxylin-eosin (HE) staining. Images were captured with a Zeiss Axiophot microscope with a Plan-NEOFLUAR 10x/0.3 objective (Zeiss, Oberkochen, Germany) and a DP70 camera (Olympus, Southend-on-Sea, UK). To avoid specific biases due to potential differences in lesion shape, cross sections of the entire lesion were analysed and averaged.

To obtain the aortas for the analysis, after fixing in PFA overnight at 4° C, the aortas were whole-mount stained with 0.2% Oil Red O (ORO, Sigma, St. Louis, MO, USA) in 80% methanol, opened longitudinally and pinned to black wax to expose the entire luminal surface. Images were acquired using a Leica MZ6 SZX10 stereomicroscope (Leica Microsystems, Wetzlar, Germany) coupled to a Leica DFC300 digital colour camera (Leica Microsystems, Wetzlar, Germany). The planimetric area of atherosclerotic plaques was measured in pixels using ImageJ.

Immunostaining

Human arteries were fixed overnight in 4 % paraformaldehyde/0.1 M PBS (pH 7.4), embedded in paraffin and sectioned into 5 µm sections with a microtome (Jung RM2055, Leica, Wetzlar, Germany). Deparaffinised sections were rehydrated, subjected to antigen retrieval in 10 mM citrate buffer pH 6.0,

blocked and incubated with a rabbit polyclonal antibody against NOD1 (1:40, Abcam, Cambridge, UK). After extensive washes, sections were incubated with a biotinylated goat anti-rabbit secondary antibody (Vector, Burlingame, CA, USA). Immunocomplexes were detected after incubation with Vectastain Elite ABC reagent (PK6100, Vector, Burlingame, CA, USA) and DAB substrate (Roche, Basel, Switzerland). Images were acquired with an Olympus Vanox AHBT3 microscope and digitalised by a Sony camera (DXC-S500).

For immunostaining of cryo-section samples and endothelial cells, slides were stained with antibodies specific for mouse CD31 (1:100, BD Biosciences, San Jose, CA, USA), CD54 (1:100, BD Biosciences, San Jose, CA, USA), CD68 (1:200, Abcam, Cambridge, UK), Ly6G (1:100, BD Biosciences, San Jose, CA, USA), NF-κB p65 (1:100, Santa Cruz, Dallas, Texas, USA) and VCAM-1 (1:100, R&D Systems, Minneapolis, MN, USA), followed by secondary staining using standard procedures. Secondary antibodies for immunofluorescence were Alexa Fluor 647-conjugated anti-rabbit (Invitrogen, Waltham, MA, USA), Alexa Fluor 594-conjugated anti-rat (Invitrogen, Waltham, MA, USA), FITC-conjugated anti-mouse (Sigma, St. Louis, MO, USA) and Cy3-conjugated anti-Armenian hamster (Jackson ImmunoResearch Laboratories, Cambridgeshire, UK). Nuclei were counterstained with DAPI (Life Technologies, Waltham, MA, USA). Immunofluorescence staining of cryo-sections were mounted in Prolong Gold Antifade mounting medium (Life Technologies, Waltham, MA, USA). Primary control panel was performed with an appropriate isotype control IgG and secondary controls incubations were performed in the absence of primary antibody.

A LSM710 confocal microscope with a Plan-APOCHROMAT 25x/0.8 oil immersion objective (Zeiss, Oberkochen, Germany) was used to capture images from immunofluorescence staining. Images were analysed using ImageJ and were processed for presentation with Zen2009 software.

^{18}F-FDG PET/CT imaging

^{18}F-FDG PET/CT images were acquired by using combined modality PET/CT as previously described (14). Briefly, ^{18}F-FDG (37 MBq/kg; 0.2 mL) was administered intraperitoneally in overnight starved animals. PET/CT imaging was performed in animals under general anaesthesia (inhalant isoflurane, Abbott Laboratories, Illinois, USA) in an INVEON microCT-microSPECT-microPET (Siemens, Munich, germany) system for small animals.

The parameter for the relative measure of FDG uptake was the standardized uptake value (SUV). The target-to-background ratio (TBR) was calculated as a quotient between the maximum SUV (SUV_{max}) of 5 regions of interest in the descending aorta corrected by mean SUV in the reference tissue (paraspinus muscle on the axial view).

Flow cytometry

To characterise leukocyte populations in $Apoe^{-/-}Nod1^{-/-}$ and $Apoe^{-/-}$ vasculature, mechanically-digested adventitia-free aortas were immersed in Aorta Dissociation Enzyme Solution (ADES; 395U/ml type II collagenase, 0.744 U/ml elastase) for 30 min at 37ºC. Single cell suspensions were prepared by passing the resulting solution through a 70 µm cell strainer. After 400g centrifugation for 5 min at 4ºC, pellet was resuspended in Hank's Balanced Salt Solution (HBSS, Gibco, Waltham, MA, USA) supplemented with 10 mM Hepes and BSA 0.5% (pH 7.4), and incubated for 30 min at 4ºC with rat APC-Cy7-conjugated monoclonal antibody against CD45 (1:200, Biolegend, San Diego, CA, USA), rat PE-conjugated monoclonal antibody against CD115 (1:100, Invitrogen, Waltham, MA, USA), rat PerCpCy5.5-conjugated monoclonal antibody against Ly6G (1:100, Biolegend, San Diego, CA, USA), rat FITC-conjugated monoclonal antibody against Ly6C (1:100, Biolegend, San Diego, CA, USA) and rat APC-conjugated monoclonal antibody against F4/80 (1:100, Biolegend, San Diego, CA, USA). For cell counting, absolute counting beads were used (CountBright^{TM}, Invitrogen, Waltham, MA, USA).

Flow cytometry was conducted in a FACSCanto II (Beckton Dickinson, Franklin Lakes, NJ, USA) and leukocyte subsets were defined using FlowJo software (Tree Star, Ashland, OR, USA): neutrophils (CD45$^+$CD115$^-$Ly6G$^+$), inflammatory monocytes (CD45$^+$CD115$^+$ Ly6C$^+$) and tissue macrophages (CD45$^+$CD115$^-$F4/80$^+$).

Bone marrow transplantation

Bone marrow (BM) transplantation was performed as previously described (15). Briefly, 8 weeks-old male $Apoe^{-/-}$ and $Apoe^{-/-}Nod1^{-/-}$ mice were irradiated (two same-day doses of 4.5 Gy) and transplanted by intravenous injection through the orbital vein under general anaesthesia of the animal (inhalant isoflurane, Abbott Laboratories). Bone marrow-derived cells (10^7) were obtained from tibias and femurs of euthanized donors $Apoe^{-/-}$ or $Apoe^{-/-}Nod1^{-/-}$ mice giving four groups: $Apoe^{-/-}$ BM -> $Apoe^{-/-}$; $Apoe^{-/-}$ BM -> $Apoe^{-/-}Nod1^{-/-}$; $Apoe^{-/-}Nod1^{-/-}$ BM -> $Apoe^{-/-}Nod1^{-/-}$; $Apoe^{-/-}Nod1^{-/-}$ BM -> $Apoe^{-/-}$. After 6 weeks on chow diet, transplanted mice were placed on HFD for 3 weeks. Successful engraftment was confirmed by PCR (data not shown).

Intravital microscopy

Leukocyte-endothelial interactions along the carotid artery and the cremaster microcirculation were analysed in $Apoe^{-/-}Nod1^{-/-}$ and $Apoe^{-/-}$ mice that received high-fat diet for 3 weeks. For VCAM-1 blocking studies *in vivo*, and prior to recording, mice were pre-treated with 100 µg/mice C12-iE-DAP or iE-Lys (Invivogen, San Diego, CA, USA) for 24 hours and then treated with 1 mg/kg mice BIO 5192 (Tocris Bioscience, Bristol, UK) for other 24 hours. The blood flow from alive animals was recorded under general anaesthesia of the mice (ketamine/xylazine combination at 100 mg/kg mice and 10 mg/kg mice, respectively).

Cremaster surgical exposure was performed as previously described (16). Briefly, once exteriorised, it was placed onto an optical clear viewing pedestal, cut longitudinally with a high temperature surgical

cautery (Lifeline Medical, Framingham, MA, USA) and held extended at the corners of the exposed tissue using surgical suture. For intravital microscopy in the carotid artery, mice were placed in supine position, and the right jugular vein was cannulated with a catheter (PE10, Becton Dickinson, Franklin Lakes, NJ, USA) for antibody injection.

10 min prior to start recording the videos, antibodies (at 0.5 µg) against Ly6C (Biolegend, San Diego, CA, USA), Ly6G (Biolegend, San Diego, CA, USA) and CD11b (eBioscience, Waltham, MA, USA) were injected to label myeloid cell subsets.

To maintain the correct temperature and physiological conditions, the exposed tissues were perfused continuously with 37° C pre-warmed Tyrode's buffer solution (139 mM NaCl, 3 mM KCl, 17 mM NaHCO$_3$, 12 mM Glucose, 3 mM CaCl$_2$ and 1 mM MgCl$_2$).
The cremasteric microcirculation was observed using a AXIO Examiner Z.1 work station (Zeiss, Oberkochen, Germany) mounted on a 3-dimensional motorized stage (Sutter Instrument, Novato, CA, USA) and equipped with a CoolSnap HQ2 camera (Photometrics, Huntington Beach, CA, USA). The objective used is an APO 20x NA 1.0 water-immersion objective. Slidebook software 5.0 (Intelligent Imaging Innovations, London, UK) was employed for acquisition and image processing. Three randomly-selected arterioles and venules were analysed per mouse, and monocytes/neutrophils were considered adherent when no rolling was observed using a reference line perpendicular to blood flow for at least 30 seconds.

Carotid intravital microscopy was performed using a BX51 microscope (Olympus, Southend-on-Sea, UK) equipped with a 9100-02 EMCCD camera (Hamamatsu Photonics, Shizuoka, Japan) and a 10x saline immersion objective. For image acquisition and analysis Olympus Cell R software was used. Leukocyte adhesion was measured as described for the cremaster for 5 min.

Plasma lipoprotein analysis

Whole blood was extracted *post-mortem* by cardiac puncture and plasma was obtained by centrifugation at 2000g during 10 min at 4° C. Plasma concentrations of total cholesterol, free cholesterol, LDL-cholesterol, HDL-cholesterol and triglycerides were measured enzymatically using Kinetic colorimetric kits (Spinreact, Girona, Spain) according to manufacturer's instructions. Mouse inflammatory mediators were quantified in plasma using the Milliplex™ Map Mouse Cytokine/Chemokine Magnetic Bead Panel (Merck Millipore, Ontario, Toronto, Canada) including interleukin 1β, 6 and tumour necrosis factor-α (TNFα), in a Luminex™ 100 IS system (Austin, Texas, USA) as per manufacturer's specifications.

Quantification and statistical analysis

All values are expressed as means ± s.e.m. Statistical calculations were performed using GraphPad Prism 6 (GraphPad Software Inc., San Diego, CA, USA). After calculating for normality by D'Agostino-Pearson omnibus test, either a non-parametric test (Mann-Whitney U-test), or a normality test (unpaired Student's t test with Welch's correction, ordinary one-way ANOVA) was used as appropriate. Statistical

significance was deemed at p values <0.05. Removal of outliers was assessed by ROUT method. Statistical tests and p values are specified for each panel in the respective figure legends. *n* indicated in the figure legends refers to the number of individual animals for *in vivo* and *ex vivo* assays.

RESULTS

Endothelial NOD1 is upregulated in atherosclerotic human arteries and its genetic deletion prevents early atherosclerosis development in *Apoe*^{-/-} mice

To evaluate the importance of NOD1 activation in human atherosclerosis, we compared atherosclerotic coronary arteries with non-atherosclerotic arteries. NOD1 and pRIP2 protein expression was markedly higher in atherosclerotic vessels than in non-atherosclerotic coronary arteries, as revealed by Western blot analysis (**Fig. 1a**).

We also examined the upstream signalling cascade of NOD receptors in the aortic lesions of *Wt* and *Apoe*^{-/-} mice fed high-fat diet (HFD) for 3 weeks. *Nod1* mRNA expression in *Apoe*^{-/-} aortas showed 5-fold induction *vs.* non-atherosclerotic aortas (**Fig. 1b**); however, *Nod2* mRNA levels were unaffected (**Fig. S1**). Differences in atherosclerotic condition regarding *Nod1* induction, but not *Nod2*, were accompanied by correspondingly higher levels of RIP2 phosphorylation in *Apoe*^{-/-} mice (**Fig. 1c**).

To investigate the contribution of NOD1 to atheroma formation, we compared *Apoe*^{-/-} *vs. Apoe*^{-/-}*Nod1*^{-/-} mice after 3 weeks on HFD. No significant differences between *Apoe*^{-/-} and *Apoe*^{-/-}*Nod1*^{-/-} mice were observed in body weights, pro-inflammatory cytokine profile (**Fig. S2**), plasma concentrations of triglycerides, total and free cholesterol, as well as HDL and LDL levels (**Table S1**). However, haematoxylin-eosin (HE) staining of aortic sinus cross-sections revealed a significantly smaller lesion area in *Apoe*^{-/-}*Nod1*^{-/-} mice compared to *Apoe*^{-/-} mice (**Fig. 1d**). Accordingly, evaluation of ^{18}F-FDG incorporation and Oil Red O (ORO)-stained lesion area revealed a significant decrease on disease progression in the aorta of *Apoe*^{-/-}*Nod1*^{-/-} mice compared to *Apoe*^{-/-} mice (**Fig. 1e, f**). Similarly, decreased amounts of plaque leukocytes correlating with a decreased accumulation of tissue F4/80[+] macrophages and Ly6G^{+} neutrophils were found in *Apoe*^{-/-}*Nod1*^{-/-} *vs. Apoe*^{-/-} vasculature (**Fig. 1g, S3**). Altogether, these results indicate that *Nod1* deficiency inhibits the onset of atherosclerosis by reducing the infiltration of myeloid cells to the early atheroma.

To further examine the role of *Nod1* in atherosclerosis, we performed bone marrow (BM) transplantation in *Apoe*^{-/-} and *Apoe*^{-/-}*Nod1*^{-/-} mice. HE staining revealed larger lesions in chimeric *Apoe*^{-/-} mice transplanted with *Apoe*^{-/-} or *Apoe*^{-/-}*Nod1*^{-/-} BM cells than in *Apoe*^{-/-}*Nod1*^{-/-} mice transplanted with either *Apoe*^{-/-} or *Apoe*^{-/-}*Nod1*^{-/-} BM, suggesting that NOD1 expression in BM-derived cells is not critical for atherosclerosis progression (**Fig. 1h**). Consistent with the importance of non-hematopoietic NOD1 in early atherosclerosis, the total content of CD68^{+} and Ly6G^{+} cells in the aortic sinus of *Apoe*^{-/-} mice, was significantly reduced in *Apoe*^{-/-}*Nod1*^{-/-} mice transplanted with either *Apoe*^{-/-} or *Apoe*^{-/-}*Nod1*^{-/-} BM cells (**Fig. 1i**). Of note, human atherosclerotic lesions showed marked NOD1 staining in the endothelial layer compared to non-atherosclerotic coronary arteries (**Fig. 1j**), suggesting that NOD1 may play a crucial role in the endothelial dysfunction that precedes the sequential recruitment of circulating platelets, neutrophils and monocytes to the intima in early stages of atherogenesis (17).

NOD1 modulates endothelial VCAM-1 as an autocrine response to danger signals

Ig-CAMs expressed by ECs bind to leukocyte integrins and participate in leukocyte adhesion to the inflamed vasculature. Immunohistochemical staining in the aortic valve revealed significantly reduced expression of the adhesion molecule VCAM-1, but not ICAM-1 nor PECAM-1, in the endothelium of fat-fed *Apoe*^{-/-}*Nod1*^{-/-} lesions compared to those on *Apoe*^{-/-} mice (**Fig. 2a**). These data suggest a role for endothelial NOD1 in promoting inflammatory cell infiltration by sustaining the expression of VCAM-1 in the context of atherosclerosis.

The stimuli most commonly used to induce VCAM-1 expression in vascular ECs is TNF-α. However, further conceivably inflammatory stimuli that accentuate atherogenesis might not only be microbial agents (18), where NODs play a major role, but also lipid products (19), where the best-investigated effector signal is oxLDL. Therefore, through VCAM-1 immunofluorescence staining we tested straightforward the response of endothelial NOD1 to these danger signals.

Not surprisingly, mouse lung endothelial cells (MLECs) from both *Apoe*^{-/-} and *Apoe*^{-/-}*Nod1*^{-/-} mice upregulated VCAM-1 expression when challenged with TNF-α compared to non-treated controls (**Fig. 2b**). This effect was maintained in *Apoe*^{-/-} MLECs after pharmacological activation of NOD1 with the selective ligand c12-iE-DAP, but not with the negative control iE-Lys (**Fig. 2b**). Interestingly, VCAM-1 upregulation was prevented in both *Apoe*^{-/-}*Nod1*^{-/-} MLECs and in *Apoe*^{-/-} MLECs treated with nodinitib-1 to inhibit NOD1. These findings confirm c12-iE-DAP as a specific agonist for NOD1 and demonstrate a major role for NOD1 in the endothelial expression of VCAM-1.

oxLDLs are potent inducers of ECAM expression in early atherosclerosis (20, 21). We found increased VCAM-1 expression in *Apoe*^{-/-} MLECs incubated with oxLDL compared to *Apoe*^{-/-} and *Apoe*^{-/-}*Nod1*^{-/-} MLECs treated with native LDL (**Fig. 2b**). However, oxLDL-induced VCAM-1 expression was significantly reduced to control levels in *Apoe*^{-/-}*Nod1*^{-/-} or nodinitib-1 pre-treated *Apoe*^{-/-} MLECs (**Fig. 2b**). Thus, NOD1 is required for oxLDL-triggered endothelial VCAM1 expression.

NOD1 signalling pathway involves NF-κB activation, which in turn promotes *Vcam1* gene expression. We confirmed that in presence of PGN and oxLDL, NOD1 triggers translocation of NF-κB to the nucleus (**Fig. 2c**) and hence the transcription of *Vcam1* is promoted (**Fig. 2d**). Similarly, pre-treatment of *Apoe*^{-/-} MLECs with GSK583 to inhibit RIP2 activity, prevented the expression of VCAM-1 following stimulation with both oxLDL and c12-iE-DAP (**Figure 2d**), further demonstrating the importance of the NOD1-RIP2-NF-κB signalling cascade that mediates VCAM-1 upregulation in ECs in response to these danger signals. In ECs, the lectin-like oxLDL receptor-1 (LOX1) has been suggested to internalize oxLDL (22). Hence, we pre-treated *Apoe*^{-/-} MLECs with a neutralizing antibody against LOX1 receptor (**Fig. 2d, upper panel**). Blockade of LOX1 prevented VCAM-1 expression in oxLDL-treated *Apoe*^{-/-} MLECs. These results were accompanied by correspondingly decreases in RIP2 and NF-κB activations (**Fig. S4**). Given no

statistical differences in *Lox1* expression in the aortic arches of *Apoe*^{-/-}*Nod1*^{-/-} and *Apoe*^{-/-} mice (**Fig. S5**), we suggest LOX1 as the endothelial receptor that allows oxLDL transduce the signal to cytoplasmic NOD1.

To refine this cellular mechanistic link between NOD1 and VCAM-1, we performed cell co-culture experiments to assess whether this interplay was dependent on intrinsic or extrinsic cell mediators. Interestingly, our results show that in the oxLDL-mediated response, only supernatants produced by *Nod1*^{+/+} MLECs induce VCAM-1 expression, regardless the MLEC genotype. However, the iE-DAP response requires the presence of NOD1 in both stimulated and supernantant-producing MLECs to significantly increase VCAM-1 expression (**Figure 2e**), highlighting anew the selectivity of the chemical agonist c12-iE-DAP in the NOD1-mediated specific response. To further confirm this NOD1-autocrine signalling mechanism, we analysed RIP2 and NF-κB activations in *Wt* and *Nod1*^{-/-} MLECs stimulated for 24h with supernatant produced by *Wt* MLECs in response to oxLDL and c12-iE-DAP (**Fig. 2f**). Interestingly enough, while oxLDL-intermediate metabolite (Ω, **Fig. 2g**) activates VCAM-1 protein expression through NF-κB in a non-NOD1-dependent manner, NOD1 presence is mandatory in both the production and the signalling through peptidoglycan-derived metabolite (δ, **Fig. 2g**).

Taken together, our results unveil pro-atherogenic oxLDL and bacterial PGNs as paramount NOD1 activity regulators that mediate in an autocrine manner, the induction of VCAM-1 expression in ECs through the RIP2 and NF-κB signalling cascade (**Figure 2g**), promoting leukocyte recruitment into the vessel wall during atherosclerosis development.

Nod1 controls leukocyte recruitment to the micro- and macro-circulation

To assess the importance of NOD1 during leukocyte adhesion we performed intravital microscopy in the cremaster muscle and the carotid artery of *Apoe*^{-/-} and *Apoe*^{-/-} *Nod1*^{-/-} mice fed HFD for 3 weeks. Compared to *Apoe*^{-/-} mice, we found reduced adhesion of both Ly6C- and Ly6G-labeled leukocytes in *Apoe*^{-/-}*Nod1*^{-/-} post-capillary venules (**Fig. 3a**). Although NOD1 activation upon treatment with c12-iE-DAP significantly increased the adhesion of both leukocytes subsets to the cremasteric vasculature in *Apoe*^{-/-} mice, treatment with BIO 5192 to selectively inhibit the integrin VLA-4 completely reversed the c12-iE-DAP effect on leukocyte adhesion (**Fig. 3b**), suggesting a relevant link between NOD1 and VCAM-1 in leukocyte recruitment to the microvasculature. In line with these results, the adhesion of Ly6C^{+} monocytes and Ly6G^{+} neutrophils to the carotid bifurcation in *Apoe*^{-/-}*Nod1*^{-/-} mice was also significantly diminished compared to *Apoe*^{-/-} mice (**Fig. 3c**). Furthermore, injection of an anti-CD11b antibody revealed that most of these adherent cells were inflammatory myeloid cells (**Fig. S6**), highlighting the substantial importance of the genetic ablation of *Nod1* on impairing peripheral blood leukocyte recruitment to the circulatory system.

DISCUSSION

In the present study, we assessed the role of NOD1 in the early atherosclerosis development. Our results demonstrate that NOD1 expression is induced in murine and human atherosclerotic tissues and strongly suggest that NOD1 participates in the initial endothelial dysfunction associated to atherosclerosis. In addition, we have identified several mechanisms involving endothelial NOD1 activation. In particular, we have shown that NOD1 mediates monocyte and neutrophil infiltration into atheromatous lesions through the autocrine regulation of endothelial VCAM-1 expression. We here also demonstrate that similar to PGNs, oxLDLs upregulate in an autocrine manner, the expression of VCAM-1 in ECs through the canonical NOD1 signalling pathway that includes RIP2 and NF-κB proteins. This early activation of endothelial NOD1 contributes to the vascular dysfunction preceding atherosclerosis progression *in vivo* (**Fig. 3d**).

So far, only a limited number of studies *in vivo* have shown the effect of NOD1 in the cardiovascular field (23–26). Consistent with a previous report (27), we here establish that *Nod1* deficiency prevents early atherosclerosis development in *Apoe⁻/⁻* mice. Although human and murine atherosclerosis differ in several aspects, critical features are shared. Our findings indicate that one such feature is NOD1 activation in the endothelium, suggesting prognostic value in atherosclerosis progression to the prompt detection of endothelial NOD1 activation (28–30). Actually, EC injury during atherogenesis triggers leukocyte infiltration through upregulation of ECAMs (31). In this regard, VCAM-1 expression has been shown to be stimulated in response to bacterial components in human ECs through the TLR2/4 signalling pathway (32–34), as well as through NOD1/2 in periodontal fibroblasts (35). In agreement with these observations, our findings provide evidence for endothelial NOD1 in directing the expression of VCAM-1 in the inflamed vessel wall. Even though endogenous NOD1/2 ligands are still unknown, here we also unveil new mediators of NOD1 activity. Actually, upon oxLDL endothelial uptake through LOX1, NOD1 classical signalling pathway (36) is activated and modulates the expression of VCAM-1 in a cell extrinsic way alike PGNs. To date, the most studied autocrine signalling loop in vascular endothelium is mediated by the soluble vascular endothelial growth factor (VEGF) (37), also known to activate the expression of VCAM-1 mainly through NF-κB (38). However, no association between VEGF and NOD1 has been established yet. Thus, extensive research on VEGF and other mediators will be required to decipher the autocrine function of the vascular endothelium in the innate response mediated by NOD1.

Exposure to different shear stress forces makes arterial and microvascular ECs display singular patterns on cell surface components (39–41). However, our intravital microscopy imaging studies in both cremaster muscle and carotid artery bifurcation in *Apoe⁻/⁻* mice yield consistent results concerning NOD1. The novel and imperative role of NOD1 in firm leukocyte adhesion to the inflamed endothelia extends the significance of the herein identified process to other arterial pathologies such as peripheral vascular disease, aneurysm formation or arteritis (42–44).

15

Dysfunction of the arterial endothelium is important not only at the inception of the atherosclerotic lesion, but at every stage in plaque development, including the events surrounding plaque rupture. Thus, NOD1 constitutes a potential therapeutic target not only for the blockade of atherosclerosis, but also for other diseases where the endothelium plays a key role such as the pathogenesis of sepsis and its sequelae. Future development of strategies aimed at local or arterial endothelial-specific neutralization of NOD1, may open new therapeutic approaches for the prevention and treatment of atherosclerosis either alone or in combination with standard treatments.

ACKNOWLEDGEMENTS

AUTHOR CONTRIBUTIONS

S.G.-R. designed the study, performed experiments, analysed data, and wrote the paper. M.P.-G., C.R., A. del M.-M., C.R., V.F.-G. performed experiments and analysed data. MA. L. provided native LDL and ox-LDL; J.M.-G. provided clinical samples; P.M.-S. provided intellectual input. V.A. provided intellectual input, funding and revised the manuscript. O.S. performed experiments, analysed data, wrote the paper, provided funding and intellectual input. L.B. designed the study, provided funding and wrote the manuscript.

REFERENCES

1. Brown, R. A., Shantsila, E., Varma, C., and Lip, G. Y. H. (2017) Current Understanding of Atherogenesis. *Am. J. Med.* **130**, 268–282

2. Schmidt, E. P., Kuebler, W. M., Lee, W. L., and Downey, G. P. (2016) Adhesion molecules: Master controllers of the circulatory system. *Compr. Physiol.* **6**, 945–973

3. Glass, C. K. and Witztum, J. L. (2001) Atherosclerosis : The Road Ahead. *Cell* **104**, 503–516

4. Zimmer, S., Grebe, A., and Latz, E. (2015) Danger signaling in atherosclerosis. *Circ. Res.* **116**, 323–340

5. Girardin, S. E., Boneca, I. G., Carneiro, L. A. M., Antignac, A., Jéhanno, M., Viaja, J., Tedin, K., Taha, M.-K., Labigne, A., Zähringer, U., Coyle, A. J., DiStefano, P. S., Bertin, J., Sansonetti, P. J., and Philpott, D. J. (2003) Nod1 Detects a Unique Muropeptide from Gram-Negative Bacterial Peptidoglycan. *Science (80-.).* **300**, 1584–1587

6. Kobayashi, K., Inohara, N., Hernandez, L. D., Galan, J. E., Nunez, G., Janeway, C. A., Medzhitov, R., and Flavell, R. A. (2002) RICK/Rip2/CARDIAK mediates signalling for receptors of the innate and adaptive immune systems. *Nature* **416**, 194–199

7. Hasegawa, M., Fujimoto, Y., Lucas, P. C., Nakano, H., Fukase, K., Núñez, G., and Inohara, N. (2008) A critical role of RICK/RIP2 polyubiquitination in Nod-induced NF-kappaB activation. *EMBO J.* **27**, 373–383

8. Viala, J., Chaput, C., Boneca, I. G., Cardona, A., Girardin, S. E., Moran, A. P., Athman, R., Memet, S., Huerre, M. R., Coyle, A. J., DiStefano, P. S., Sansonetti, P. J., Labigne, A., Bertin, J., Philpott, D. J., and Ferrero, R. L. (2004) Nod1 responds to peptidoglycan delivered by the Helicobacter pylori cag pathogenicity island. *Nat. Immunol.* **5**, 1166–1174

9. Zhang, S. H., Reddick, R. L., Piedrahita, J. A., and Maeda, N. (1992) Spontaneous hypercholesterolemia and arterial lesions in mice lacking apolipoprotein E. *Science (80-.).* **258**, 468–471

10. Plump, A. S., Smith, J. D., Hayek, T., Aalto-Setälä, K., Walsh, A., Verstuyft, J. G., Rubin, E. M., and Breslow, J. L. (1992) Severe hypercholesterolemia and atherosclerosis in apolipoprotein E-deficient mice created by homologous recombination in ES cells. *Cell* **71**, 343–353

11. Chamaillard, M., Hashimoto, M., Horie, Y., Masumoto, J., Qiu, S., Saab, L., Ogura, Y., Kawasaki, A., Fukase, K., Kusumoto, S., Valvano, M. A., Foster, S. J., Mak, T. W., Nuñez, G., and Inohara, N. (2003) An essential role for NOD1 in host recognition of bacterial peptidoglycan containing diaminopimelic acid. *Nat. Immunol.* **4**, 702–707

12. Luque, A., Carpizo, D. R., and Iruela-arispe, M. L. (2003) ADAMTS1 / METH1 Inhibits Endothelial Cell Proliferation by Direct Binding and Sequestration of VEGF 165. *J. Biol. Chem.* **278**, 23656–23665

13. Fuster, J. J., González-Navarro, H., Vinué, A., Molina-Sànchez, P., Andrés-Manzano, M. J., Nakayama, K. I., Nakayama, K., Díez-Juan, A., Bernad, A., Rodríguez, C., Martínez-González, J., and Andrés, V. (2011) Deficient p27 phosphorylation at serine 10 increases macrophage foam cell formation and aggravates atherosclerosis through a proliferation-independent mechanism. *Arterioscler. Thromb. Vasc. Biol.* **31**, 2455–2463

14. Fueger, B. J., Czernin, J., Hildebrandt, I., Tran, C., Halpern, B. S., Stout, D., Phelps, M. E., and Weber, W. A. (2006) Impact of Animal Handling on the Results of 18 F-FDG PET Studies in Mice. *J. Nucl. Med.* **47**, 999–1007

15. Lichtenstein, L., Serhan, N., Espinosa-delgado, S., Annema, W., Tietge, U. J. F., Robaye, B., Boeynaems, J., Laffargue, M., Perret, B., and Martinez, L. O. (2015) Increased atherosclerosis in P2Y 13 / apolipoprotein E double-knockout mice : contribution of P2Y 13 to reverse cholesterol transport. *Cardiovasc. Res.* **106**, 314–323

16. Rius, C. and Sanz, M. J. (2015) Intravital Microscopy in the Cremaster Muscle Microcirculation for Endothelial Dysfunction Studies. *Methods Mol. Biol.* **1339**, 357–366

17. Swirski, F. K. and Robbins, C. S. (2013) Neutrophils usher monocytes into sites of inflammation. *Circ. Res.* **112**, 744–745

18. Jonsson, A. L. and Bäckhed, F. (2017) Role of gut microbiota in atherosclerosis. *Nat. Rev. Cardiol.* **14**, 79–87

19. Gimbrone, M. A. and García-Cardeña, G. (2016) Endothelial Cell Dysfunction and the Pathobiology of Atherosclerosis. *Circ. Res.* **118**, 620–636

20. Cai, H. and Harrison, D. G. (2000) Endothelial dysfunction in cardiovascular diseases: the role of oxidant stress. *Circ. Res.* **87**, 840–844

21. Libby, P., Ridker, P. M., and Maseri, A. (2002) Inflammation and atherosclerosis. *Circulation* **105**, 1135–1143

22. Pirillo, A., Norata, G. D., and Catapano, A. L. (2013) LOX-1, OxLDL, and atherosclerosis. *Mediators Inflamm.* **2013**

23. Prieto, P., Vallejo-Cremades, M. T., Benito, G., González-Peramato, P., Francés, D., Agra, N., Terrón, V., Gónzalez-Ramos, S., Delgado, C., Ruiz-Gayo, M., Pacheco, I., Velasco-Martín, J. P., Regadera, J., Martín-Sanz, P., López-Collazo, E., Boscá, L., and Fernández-Velasco, M. (2014) NOD1 receptor is up-regulated in diabetic human and murine myocardium. *Clin. Sci.* **127**, 665–677

24. Yang, H., Li, N., Song, L. N., Wang, L., Tian, C., Tang, C. S., Du, J., Li, H. H., Yu, X. H., and Wang, H. X. (2015) Activation of NOD1 by DAP contributes to myocardial ischemia/reperfusion injury via multiple signaling pathways. *Apoptosis* **20**, 512–522

25. Motomura, Y., Kanno, S., Asano, K., Tanaka, M., Hasegawa, Y., Katagiri, H., Saito, T., Hara, H., Nishio, H., Hara, T., and Yamasaki, S. (2015) Identification of Pathogenic Cardiac CD11c^{+} Macrophages in Nod1-Mediated Acute Coronary Arteritis. *Arterioscler. Thromb. Vasc. Biol.* **35**, 1423–1433

26. Val-Blasco, A., G.M. Piedras, M. J., Ruiz-Hurtado, G., Suárez, N., Prieto, P., González-Ramos, S., Gómez-Hurtado, N., Delgado, C., Pereira, L., Benito, G., Zaragoza, C., Domenech, N., Crespo-Leiro, M. G., Vasquez-Echeverri, D., Nuñez, G., López-Collazo, E., Boscá, L., and Fernández-Velasco, M. (2017) Role of NOD1 in Heart Failure Progression via Regulation of Ca2+ Handling. *J Am Coll Cardiol.* **69**, 423–433

27. Kanno, S., Nishio, H., Tanaka, T., Motomura, Y., Murata, K., Ihara, K., Onimaru, M., Yamasaki, S., Kono, H., Sueishi, K., and Hara, T. (2014) Activation of an Innate Immune Receptor, Nod1, Accelerates Atherogenesis in Apoe-/- Mice. *J. Immunol.* **194**, 773–780

28. Deanfield, J. E., Halcox, J. P., and Rabelink, T. J. (2007) Endothelial function and dysfunction: Testing and clinical relevance. *Circulation* **115**, 1285–1295

29. Davignon, J. and Ganz, P. (2004) Role of Endothelial Dysfunction in Atherosclerosis. *Circulation* **109**, 27–32

30. Martin, B.-J. and Anderson, T. J. (2009) Risk prediction in cardiovascular disease: the prognostic significance of endothelial dysfunction. *Can. J. Cardiol.* **25 Suppl A**, 15A–20A

31. Pober, J. S., Min, W., and Bradley, J. R. (2009) Mechanisms of Endothelial Dysfunction, Injury, and

Death. *Annu. Rev. Pathol. Mech. Dis.* **4**, 71–95

32. Zeuke, S., Ulmer, A. J., Kusumoto, S., Katus, H. A., and Heine, H. (2002) T LR4-mediated inflammatory activation of human coronary artery endothelial cells by LPS. *Cardiovasc. Res.* **56**, 126–134

33. Ogawa, H., Rafiee, P., Heidemann, J., Fisher, P. J., Johnson, N. a., Otterson, M. F., Kalyanaraman, B., Pritchard, K. a., and Binion, D. G. (2003) Mechanisms of Endotoxin Tolerance in Human Intestinal Microvascular Endothelial Cells. *J. Immunol.* **170**, 5956–5964

34. Lee, I.-T., Lin, C.-C., Hsu, C.-K., Wu, M.-Y., Cho, R.-L., and Yang, C.-M. (2014) Resveratrol inhibits Staphylococcus aureus-induced TLR2/MyD88/NF-κB-dependent VCAM-1 expression in human lung epithelial cells. *Clin. Sci.* **127**, 375–390

35. Liu, J., Wang, Y., and Ouyang, X. (2014) Beyond toll-like receptors: Porphyromonas gingivalis induces IL-6, IL-8, and VCAM-1 expression through NOD-mediated NF-kB and ERK signaling pathways in periodontal fibroblasts. *Inflammation* **37**, 522–533

36. Ogura, Y., Inohara, N., Benito, A., Chen, F. F., Yamaoka, S., and Núñez, G. (2001) Nod2, a Nod1/Apaf-1 family member that is restricted to monocytes and activates NF-kB. *J. Biol. Chem.* **276**, 4812–4818

37. Lee, S., Chen, T. T., Barber, C. L., Jordan, M. C., Murdock, J., Desai, S., Ferrara, N., Nagy, A., Roos, K. P., and Iruela-Arispe, L. M. (2007) Autocrine VEGF signaling is required for vascular homeostasis. *Cell* **130**, 691–703

38. Kim, I., Moon, S.-O., Hoon Kim, S., Jin Kim, H., Soon Koh, Y., and Young Koh, G. (2001) Vascular Endothelial Growth Factor Expression of Intercellular Adhesion Molecule 1 (ICAM-1), Vascular Cell Adhesion Molecule 1 (VCAM-1), and E-selectin through Nuclear Factor-κB Activation in Endothelial Cells. *J. Biol. Chem.* **276**, 7614–7620

39. Chiu, J. and Chien, S. (2011) Effects of disturbed flow on vascular endothelium: pathophysiological basis and clinical perspectives. *Physiol rev* **91**, 1–106

40. Aird, W. C. (2007) Phenotypic heterogeneity of the endothelium: II. Representative vascular beds. *Circ. Res.* **100**, 174–190

41. Ortega-Gómez, A., Salvermoser, M., Rossaint, J., Pick, R., Brauner, J., Lemnitzer, P., Tilgner, J., Jong, R. De, Megens, R. T. A., Jamasbi, J., Döring, Y., Pharm, C. T., Scheiermann, C., Siess, W., Drechsler, M., Weber, C., Grommes, J., Zarbock, A., Walzog, B., and Soehnlein, O. (2016) Cathepsin G Controls Arterial But Not Venular Myeloid Cell Recruitment. *Circulation* **134**, 1176–1188

42. Cid, M. C., Cebrián, M., Font, C., Coll-Vinent, B., Hernández-Rodríguez, J., Esparza, J., Urbano-Márquez, Á., and Grau, J. M. (2000) Cell adhesion molecules in the development of inflammatory infiltrates in giant cell arteritis: inflammation-induced angiogenesis as the preferential site of leukocyte-endothelial cell interactions. *Arthritis Rheum.* **43**, 184–194

43. Lee, E. S., Van Spyk, E., Chun, K., Pitts, R. L., Wu, M. H., and Yuan, S. Y. (2012) Monocytic

adhesion molecule expression and monocyte-endothelial cell dysfunction are increased in patients with peripheral vascular disease versus patients with abdominal aortic aneurysms. *J Surg Res.* **177**, 373–381

44. Gopal, K., Kumar, K., Nandini, R., Jahan, P., and Kumar, M. J. M. (2010) High fat diet containing cholesterol induce aortic aneurysm through recruitment and proliferation of circulating agranulocytes in apoE knock out mice model. *J. Thromb. Thrombolysis* **30**, 154–163

FIGURE LEGENDS

Figure 1. Endothelial NOD1 inflects vascular inflammation linked to atherosclerosis. (a) Immunoblot analysis and representative panel of NOD1 and pRIP2 in atherosclerotic (athero.) (*n*=6) and non-atherosclerotic (non-athero.) or with arterial intimal thickening (*n*=6) human coronary arteries. Protein levels were normalized to β-actin. **(b)** qRT-PCR analysis of *Nod1* in aortic arches from C57BL/6 (*Wt*; *n*=8), *Apoe*$^{-/-}$ (*n*=10) and *Apoe*$^{-/-}$*Nod1*$^{-/-}$ (*n*=8) mice fed HFD for 3 weeks. *m*RNA levels were normalized to *m18S*. **(c)** Immunoblot analysis and representative panel of pRIP2 in the same cohort. Protein levels were normalized to GAPDH. **(d)** Quantification of lesion area in the semilunar valve cups of *Apoe*$^{-/-}$ (*n*=9) and *Apoe*$^{-/-}$*Nod1*$^{-/-}$ (*n*=8) mice fed HFD for 3 weeks. **(e)** Target-to-background (TBR) ratio of arterial ^{18}F-FDG uptake in the same cohort. **(f)** Quantification of positive Oil Red O (ORO) lesion area in the indicated aortic regions in the same cohort. Panels show representative *en face* ORO staining of aortas from these animals. **(g)** Flow cytometry analysis of total number of leukocytes, macrophage, classical monocyte and neutrophil subsets in *Apoe*$^{-/-}$ (*n*=8) and *Apoe*$^{-/-}$*Nod1*$^{-/-}$ (*n*=8) mice aortas after 3 weeks on HFD. **(h)** Quantification of lesion area in the aortic sinus of *Apoe*$^{-/-}$ mice transplanted with BM from *Apoe*$^{-/-}$ (*n*=17) or *Apoe*$^{-/-}$*Nod1*$^{-/-}$ (*n*=15) mice and in *Apoe*$^{-/-}$*Nod1*$^{-/-}$ mice that underwent BM reconstitution with *Apoe*$^{-/-}$ (*n*=15) or *Apoe*$^{-/-}$*Nod1*$^{-/-}$ (*n*=16) donors as indicated. All mice groups were fed HFD for 3 weeks. **(i)** Quantification of monocyte/macrophage and neutrophil neointimal content in lesions in the aortic sinus of the same cohort. **(j)** Representative images for NOD1 immunohistochemistry in the intima of atherosclerotic (athero.) and non-atherosclerotic (non-athero.) or with arterial intimal thickening human coronary arteries. Arrows point out NOD1$^+$ cells in the vascular endothelium. Data are represented as mean ± s.e.m. of the indicated number (*n*) of repeats. *$P < 0.05$, **$P < 0.01$, ***$P < 0.001$, ****$P < 0.0001$ *vs.* non-athero. by Mann-Whitney U test **(a)**, *vs. Wt* **(b, c)** mice by one-way ANOVA, *vs. Apoe*$^{-/-}$ **(d, e, f, g)** mice by Student's *t* test and *vs. Apoe*$^{-/-}$ → *Apoe*$^{-/-}$ by one-way ANOVA **(h, i)**. $^{###}P < 0.001$ *vs. Apoe*$^{-/-}$ by Student's *t* test. *nd* = not detected. Scale bars, 100 μm **(d)**, 1 mm **(f)**, 20 μm **(j)**.

Figure 2. Bacterial peptidoglycan and oxidized LDL induce VCAM-1 expression in vascular endothelial cells through NOD1 in an autocrine manner. (a) Representative immunofluorescence images of VCAM-1, ICAM-1 and PECAM-1 staining and its corresponding perimeter quantification in lesions from the aortic sinus

of *Apoe*^{-/-} (*n*=8-14) and *Apoe*^{-/-}*Nod1*^{-/-} (*n*=8-16) mice fed HFD for 3 weeks. **(b-d)** Primary endothelial cells from *Apoe*^{-/-} (*n*=15) and *Apoe*^{-/-}*Nod1*^{-/-} (*n*=8) mice were pre-incubated with 1μM nodinitib-1, 5 μM BAY 11-7082, 5 μM GSK583 or 1μg/mL LOX1 neutralizing antibody for 1h and then exposed to 50 μg/mL oxLDL, 50 μg/mL LDL, 10 ng/mL TNF-α, 1 μg/mL iE-Lys or 1 μg/mL c12-iE-DAP for 24h. **(e)** Primary endothelial cells from *Wt* (*n*=5) and *Nod1*^{-/-} (*n*=5) mice were incubated with 50 μg/mL oxLDL, 50 μg/mL LDL, 1 μg/mL iE-Lys or 1 μg/mL c12-iE-DAP for 24h. Cell-free supernatants were transferred to a new batch of non-treated *Wt* and *Nod1*^{-/-} MLECs for 24h. Endothelial monolayers were immunostained for VCAM-1 **(b-e)** and NF-κB **(c)**. **(f)** Immunoblot analysis of pRIP2 and pNF-κB in primary endothelial cells from *Wt* (*n*=8) and *Nod1*^{-/-} (*n*=10) mice. Cell-free supernatants produced in *Wt* MLECs for 24h in presence of 50 μg/mL oxLDL or 1 μg/mL c12-iE-DAP, were transferred to a new batch of non-treated *Wt* and *Nod1*^{-/-} MLECs for 24h. Protein levels were normalized to α-tubulin. **(g)** In the presence of bacterial peptidoglycan and oxLDL, NOD1 activates RIP2 phosphorylation and secretion of yet unidentified metabolites (δ and Ω, respectively). While metabolite Ω, upon binding to a non-defined receptor (R) induces VCAM1 upregulation through NF-kB, metabolite δ upregulates VCAM1 expression in a NOD1-RIP2-NF-kB dependent manner. Blurry dotted arrows represent mechanistic hypotheses for NOD1-dependent autocrine signalling. Data is represented as mean ± s.e.m. of the indicated number (*n*) of repeats. *$P < 0.05$, **$P < 0.01$, ***$P < 0.001$, ****$P < 0.0001$ *vs. Apoe*^{-/-} **(a, b)**, BAY 11-7082 control **(d)** or *Wt* **(e, f)** by Student's *t* test **(a, b, e)** or one-way ANOVA **(d, f)**. #$P < 0.05$, ##$P < 0.01$, ###$P < 0.001$, ####$P < 0.0001$ *vs.* oxLDL **(b, d upper panel)**, c12-iE-DAP **(b, d lower panel)** or non-treated *Wt* **(e, f)** by Student's *t* test **(b, d)** or one-way ANOVA **(e, f)**. Scale bars, 50 μm **(a)**; 20 μm **(c)**.

Figure 3. Neutrophils and monocytes have impaired adhesion to the *Apoe*^{-/-}*Nod1*^{-/-} micro- and macro-circulation. Intravital microscopy imaging in the cremaster muscle **(a, b)** and carotid bifurcation **(c)** to quantify leukocyte-endothelial wall interactions 3 weeks after HFD. **(a)** Quantification and representative images of adhered Ly6C^{+} classical monocytes and Ly6G^{+} neutrophils to the cremasteric endothelium of *Apoe*^{-/-} (*n*=5-8) and *Apoe*^{-/-}*Nod1*^{-/-} (*n*=4-7) mice. **(b)** *Apoe*^{-/-} mice were injected i.v. with 100 μg of either iE-Lys (*n*=22) or c12-iE-DAP (*n*=20). The next day, and prior to the intravital microscopy recording, 1mg/kg BIO 5192 was injected i.v. to half of each group of mice. Quantification of adhered Ly6G^{+} neutrophils and Ly6C^{+} monocytes to the endothelium of each set of pre-treated *Apoe*^{-/-} mice is represented. **(c)** Quantification and representative images of adhered Ly6C^{+} monocytes and Ly6G^{+} neutrophils to the carotid bifurcation endothelium of *Apoe*^{-/-} (*n*=8) and *Apoe*^{-/-}*Nod1*^{-/-} (*n*=8) mice. The dotted lines delimit the vascular wall. **(d)** In early stages of the disease, once LDL undergoes oxidative modification in the sub-endothelial space, oxLDLs promote the expression of VCAM-1 in ECs through the cytoplasmic receptor NOD1, enabling monocyte and neutrophil recruitment to the vessel wall. Likewise, bacterial peptidoglycan (PGN)-derived peptides upon recognition by endothelial NOD1, may induce the expression of VCAM-1 that promotes leukocyte infiltration to the sub-endothelial space and subsequent plaque progression. Data are

represented as mean ± s.e.m. of the indicated number (*n*) of repeats. *$P < 0.05$, **$P < 0.01$, ***$P < 0.001$ *vs.* *Apoe*^{-/-} by Student's *t* test **(a, c)** or iE-Lys by one-way ANOVA **(b)**. [#]$P < 0.05$, [###]$P < 0.001$ *vs.* c12-iE-DAP **(b)**. Scale bar, 100μm **(a, c)**.
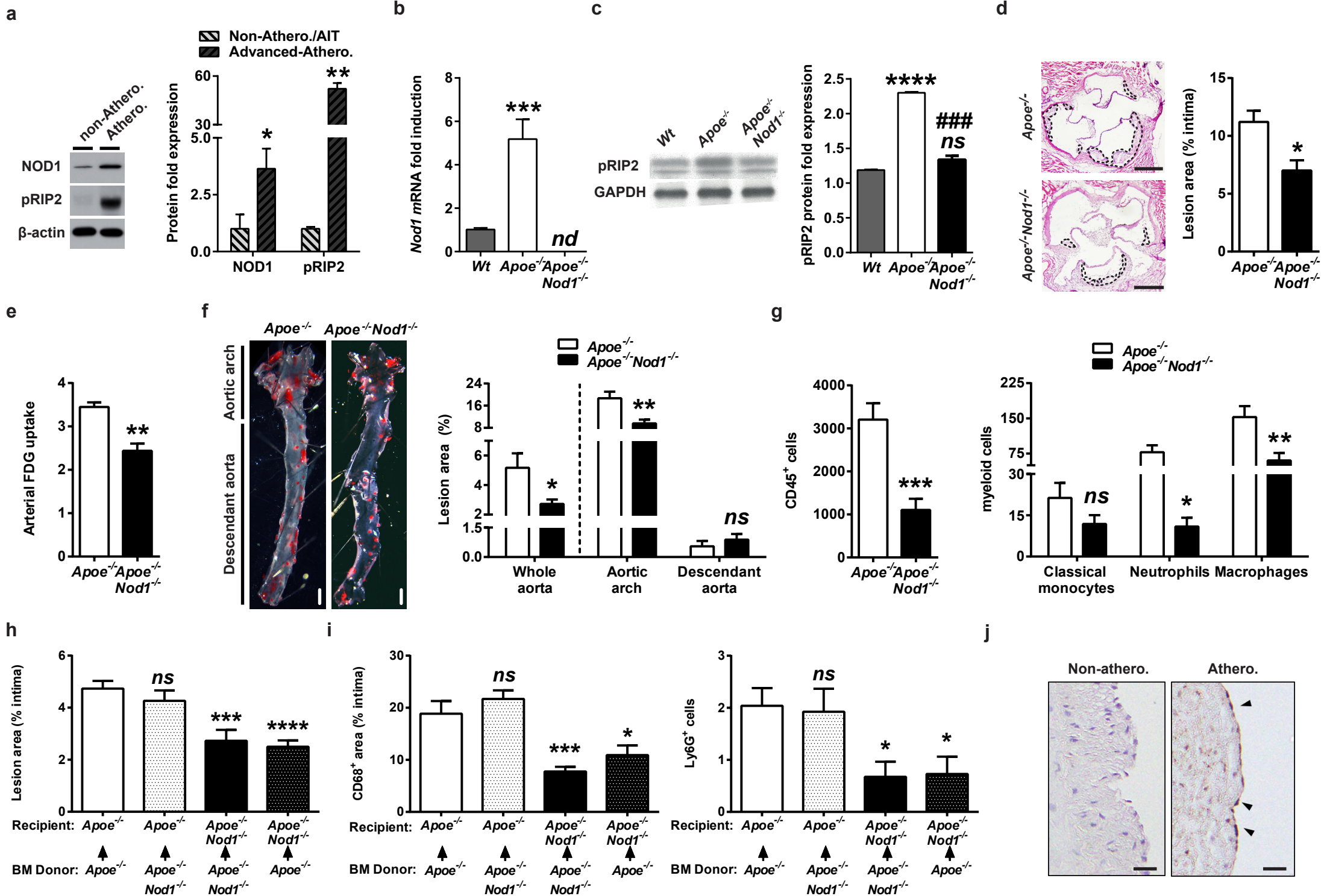
Figure 1

Figure 2

a

VCAM-1 | ICAM-1 | PECAM-1 | DAPI

Apoe^{-/-}

Apoe^{-/-}*Nod1*^{-/-}

Perimeter (% intima)

60 — 40 — 20 — 0

□ *Apoe*^{-/-} ■ *Apoe*^{-/-}*Nod1*^{-/-}

VCAM-1[+] ****
ICAM-1[+] ns
PECAM-1[+] ns

b

VCAM-1 expression/cell (% vs. control)

400 — 300 — 200 — 100 — 0

□ *Apoe*^{-/-} ■ *Apoe*^{-/-}*Nod1*^{-/-}

ns ns ns ns **** **** ns ns ns

iE-Lys	-	+	-	-	-	-	-	-
TNFα	-	-	+	-	-	-	-	-
LDL	-	-	-	+	-	-	-	-
oxLDL	-	-	-	-	+	-	-	+	-
c12-iE-DAP	-	-	-	-	-	+	-	-	+
Nodinitib-1	-	-	-	-	-	-	+	+	+

c

iE-Lys | LDL | oxLDL | c12-iE-DAP | oxLDL+ Nodinitib-1 | c12-iE-DAP+ Nodinitib-1

VCAM-1   NF-κB   DAPI

d

VCAM-1 expression/cell (% vs. control)

300 — 200 — 100 — 0

ns ns ns **** ### ### ### ns

LDL	-	-	-	+	+	-	-
oxLDL	-	+	-	-	+	+	+
GSK583	-	-	+	-	+	-	-
BAY 11-7082	+	-	-	-	-	+	-
αLOX1	-	-	-	-	-	-	+

VCAM-1 expression/cell (% vs. control)

300 — 200 — 100 — 0

ns ns **** ### ### ns

iE-Lys	-	-	+	-	-	-
c12-iE-DAP	-	-	-	+	+	+
GSK583	-	+	-	-	+	-
BAY 11-7082	+	-	-	-	-	+

e

VCAM-1 expression/cell (% vs. non-treated *Wt*)

300 — 200 — 100 — 0

■ *Wt* ■ *Nod1*^{-/-} MLEC monolayer

ns ns ns ns *** ns ns ns ns ns

φ	-	-	-	-	-	-	-	-	-
iE-Lys	-	+	-	-	-	+	-	-	-
LDL	-	-	+	-	-	-	+	-	-
oxLDL	-	-	-	+	-	-	-	+	-
c12-iE-DAP	-	-	-	-	+	-	-	-	+

Supernatant *Wt* MLECs | *Nod1*^{-/-} MLECs

f

pRIP2 protein fold expression

4 — 2 — 0

ns ns ****

φ	+	-	-
oxLDL	-	+	-
c12-iE-DAP	-	-	+

pNF-κB protein fold expression

6 — 4 — 2 — 0

■ *Wt* ■ *Nod1*^{-/-}

ns # ns **

φ	+	-	-
oxLDL	-	+	-
c12-iE-DAP	-	-	+

Wt Supernatant

g

oxLDL — LOX1 — NOD1 — RIP-2 — NF-κB — *Vcam1* — Ω
Ω — R — MEMBRANE — CYTOPLASM — NUCLEUS

PGN — NOD1 — RIP-2 — NF-κB — *Vcam1* — δ
δ — MEMBRANE — CYTOPLASM — NUCLEUS

Figure 3